A NEW METHOD FOR ATMOSPHERIC CORRECTION AND AEROSOL OPTICAL PROPERTY RETRIEVAL FOR VIS-SWIR MULTI- AND HYPERSPECTRAL IMAGING SENSORS: QUICK ATMOSPHERIC CORRECTION

Lawrence S. Bernstein,[1] Steven M. Adler-Golden,[1] Robert L. Sundberg,[1] Robert Y. Levine,[1]
Timothy C. Perkins,[1] Alexander Berk,[1] Anthony J. Ratkowski,[2] and Michael L. Hoke[2]

1.0 INTRODUCTION

A critical first step in the analysis of visible-SWIR hyperspectral or multispectral imagery (HSI or MSI) is atmospheric correction or compensation, in which atmospheric absorption and scattering effects are removed and the data are reduced to surface spectral reflectance (see Fig. 1). A number of atmospheric correction methods and algorithms exist, including algorithms based on first-principles radiation transport calculations (Gao *et al.*, 1993, 2000; Montes *et al.*, 2001; Green *et al.*, 1996; Miller, 2002; Adler-Golden *et al.*, 1999; Matthew *et al.*, 2000, 2003; Qu *et al.*, 2000; Richter and Schlaepfer, 2002), and empirical approaches such as the Empirical Line Method (ELM) (Roberts *et al.*, 1985; Kruse *et al.*, 1990), which relies on two or more known reflectances in the image. However, none of these methods provide the ideal combination of high accuracy, high computational speed, and independence from prior knowledge.

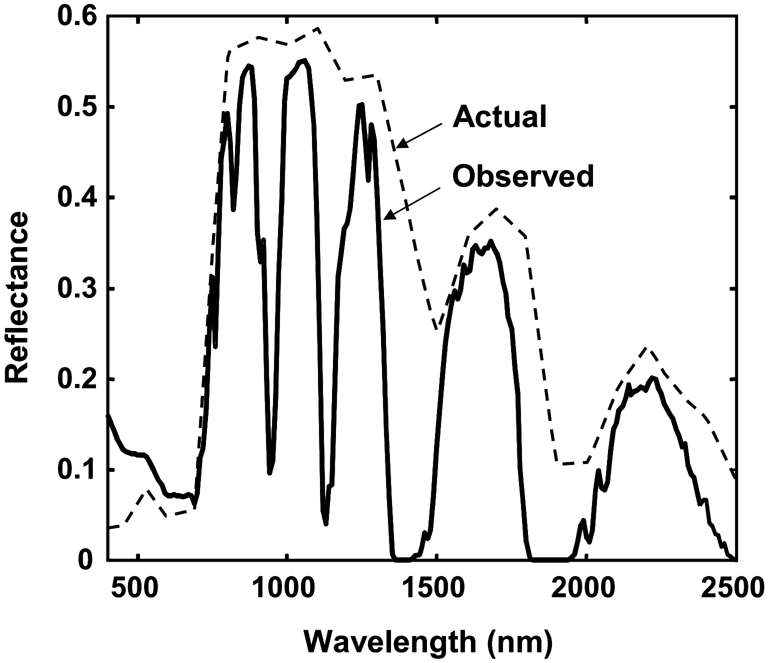

Figure 1. MODTRAN calculation of the apparent reflectance of a vegetation pixel as observed from space with nadir viewing, the Mid-Latitude Summer model atmosphere, and Rural aerosols with VIS=23km.

This paper presents a new, semi-empirical quick atmospheric correction method, dubbed QUAC, which also enables retrieval of the wavelength-dependent optical depth of the aerosol or haze and

---

[1] Spectral Sciences, Inc., 4 Fourth Avenue, Burlington, Massachusetts 01803-3304(larry@spectral.com)

[2] Air Force Research Laboratory, Hanscom Air Force Base, Massachusetts 01731-3010

molecular absorbers. It allows the retrieval of approximate reflectance spectra even when the sensor does not have a proper radiometric or wavelength calibration, or when the solar illumination intensity is unknown, such as when a cloud deck is present. Computational speed is much faster than for the first-principles methods, making it potentially suitable for real-time applications. In tests to date, QUAC has yielded remarkably good agreement with a state-of-the-art first-principles algorithm. Like the ELM, QUAC assumes a linear relationship between spectral reflectance and measured radiance, which is considered to be a good approximation for most scenes.

The standard radiance equation may be written as (Matthew *et al.*, 2000, 2003)

$$\rho_j(\lambda) = A(\lambda) + \frac{B(\lambda)}{1 - S(\lambda) < \rho(\lambda) >} \rho_j^{\mathrm{o}}(\lambda) + \frac{C(\lambda)}{1 - S(\lambda) < \rho(\lambda) >} < \rho(\lambda) > \quad \mathbf{(1)}$$

where ρ_j is the observed reflectance (the radiance normalized by the surface normal component of the solar flux) for the j'th pixel at a spectral band centered at wavelength λ. ρ_j^{o} is the actual surface reflectance, $<\rho>$ is a spatially averaged surface reflectance. A, B, C and S are coefficients that describe the transmission and scattering effects of the atmosphere. Their physical origin is highlighted in Figure 2. The first coefficient, A, accounts for light that never encounters the surface, but is scattered and absorbed within the atmosphere. The second, B, accounts for the sun-surface-sensor path direct transmittance. The third, C, accounts for diffuse transmittance and gives rise to the "adjacency effect," a spatial blending induced by atmospheric scattering. The length scale of the adjacency effect is typically of order ~0.5 km, thus $<\rho>$ is typically a slowly varying function of position within a large image. S, the atmospheric spherical albedo, accounts for enhancement of the ground illumination by atmospheric reflection.

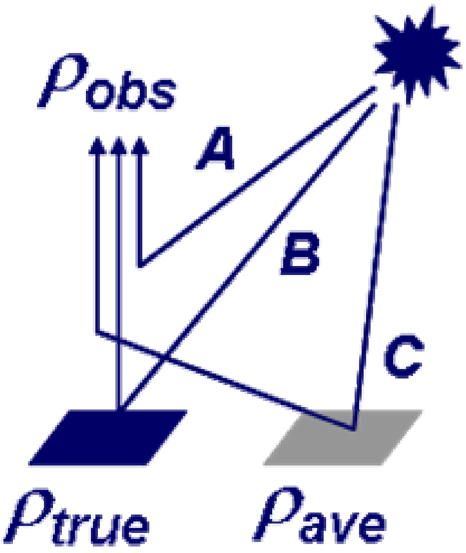

Figure 2. Radiation-transfer contributions to the observed apparent reflectance, ρ_{obs}.

Eq. (1) reduces to a linear form under many common conditions in which (1) $S<\rho>$ is small and when either, (2) the diffuse and direct transmittance terms can be combined with a single reflectance variable, or (3) the diffuse term can be combined with the backscattering term. Situation (1) occurs frequently, when the visibility is reasonably high or when the ground is dark in the visible (such as with vegetation, water, or dark soil). Situation (2) occurs when the pixels are very large, several hundred meters in size. Situation (3) occurs when the scene materials are fairly uniformly interspersed or when the image covers a small geographic area (< ~1 km), making $<\rho>$ nearly constant, or when the visibility is high, making the diffuse transmittance term small. When (1) and (3) apply, Eq. (1) reduces to the linear equation

$$\rho_j(\lambda) = A(\lambda) + B(\lambda)\rho_j^{\mathrm{o}}(\lambda) + C(\lambda) < \rho(\lambda) > \quad \mathbf{(2)}$$

With the linear Eq. (2), the aim of atmospheric compensation is essentially the determination of an offset, $A+C<\rho>$, and gain parameter, B, in order to retrieve the surface reflectance, ρ_j^{o}. Numerous approaches to this problem have been developed. The ELM assumes that the radiance image contains some pixels of known reflectance. This method is not generally applicable, as in-scene known reflectances are often not available. In variants of the ELM, approximate gain and offset values are generated using pixels in the image that are treated as if their spectra were known. For example, in the Flat Field Method a single bright pixel is taken as having a spectrally flat reflectance and the offset is taken as zero; accordingly, dividing the image pixel spectra by the bright pixel spectrum yields approximate relative reflectances. In the Internal Average Relative Reflectance method, this procedure is followed using a scene-average spectrum rather than a single bright pixel spectrum. In general, neither the Flat Field Method nor the Internal Average Relative Reflectance methods are very accurate.

First-principles methods express the Eq. (1) or Eq. (2) parameters in terms of atmospheric physical variables, such as column water vapor and aerosol optical depth or visibility. For retrieving optical depth, methods are available that rely on modeling the aerosol backscatter over "dark" pixels such as vegetation and dark soil (Kaufman *et al*., 1997) or water bodies. However, difficulties in determining the optical depth arise when there is a lack of suitable dark pixels in the scene, or when the sensor is at a low altitude, within the aerosol layer, so that the backscatter it measures is a small (and generally unknown) fraction of the total.

Like many first-principles methods, QUAC determines the atmospheric compensation parameters directly from the information contained within the scene (observed pixel spectra), without ancillary information. However, unlike most other methods, its aerosol optical depth retrieval approach does not require the presence of dark pixels. The retrieved optical depth information can therefore be utilized to improve the accuracy of methods that use first-principles modeling. In particular, it can be used to set the optical depth of a model aerosol when dark pixels are unavailable, or to select from among alternative model aerosols to provide consistency with optical depths retrieved from a dark pixel method.

2.0 QUAC ALGORITHM DESCRIPTION

The underlying assumptions of the approach are:

- There are a number ($\approx$10 or more) of diverse pixel spectra (diverse materials) in a scene,
- The spectral standard deviation of ρ_j^o for a collection of diverse materials is a nearly wavelength-independent constant, and an additional, helpful assumption is that,
- There are sufficiently dark pixels ($\rho_j^o(\lambda)\approx 0$) in a scene to allow for a good estimation of the nearly spatially invariant baseline contribution, $\rho_b = A + C\langle\rho\rangle$

The first assumption is usually applicable, as it only requires that a handful of pixels out of typically ~10^5 to 10^6 pixels display diverse spectra. The most notable exception would be a scene over completely open and deep water, in which case the material reflectance is well known *a priori*. The diverse spectra can be selected using any of a number of spectral diversity metrics and algorithms, such as endmembers. The second assumption appears to be generally true based on our empirical observation, and is likely related to the lack of spectral correlation between diverse materials. The third assumption is frequently applicable, as most scenes will contain a number of very dark pixels from such surfaces as water bodies, vegetation, and cast shadows. For the atypical cases that violate this assumption, there are alternative methods, described later, for estimating a reasonable baseline. The implementation of QUAC is straightforward and efficient, as highlighted in Figure 3. The atmospheric correction step just involves re-arranging Eq. (2) to solve for $\rho_j^o(\lambda)$ given B and the baseline. A key attribute of QUAC is its applicability to any sensor viewing or solar elevation angle.

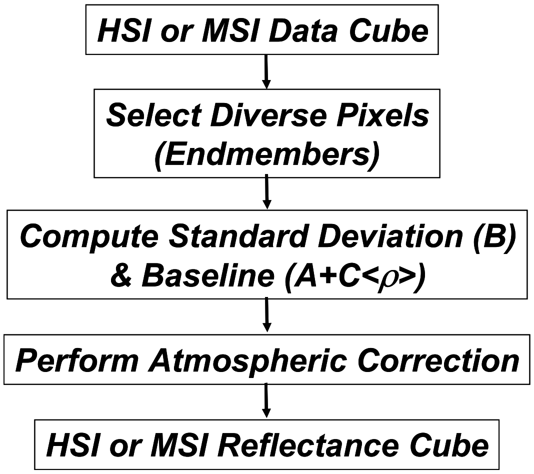

Figure 3. Overview of QUAC atmospheric correction data-processing flow.

Under the above-stated assumptions, the spectral standard deviation of Eq. (2) for a set of diverse pixel spectral can be expressed as,

$$\sigma\rho(\lambda) = B(\lambda)\sigma\rho^{0}(\lambda) \tag{3}$$

For reasons mentioned earlier, $A + C\langle\rho\rangle$ can be taken as a constant in many, if not most, cases, so it makes no contribution to the standard deviation. In cases where it varies significantly within the scene, the image can be divided into smaller pieces, as discussed below. Since $\sigma\rho^{0}$ is assumed to be spectrally invariant, then to within a normalization factor, designated g_o, $\sigma\rho$ represents the correction factor, B. The actual surface spectral reflectance can be retrieved using the extracted in-scene-determined compensation parameters and re-arrangement of Eq. (2) to yield

$$\rho_j^{0}(\lambda) = \frac{\rho_j(\lambda) - \rho_b(\lambda)}{g_o \sigma\rho(\lambda)} \tag{4}$$

where $\rho_b = A + C\langle\rho\rangle$ is the baseline contribution.

There are a number of ways in which the normalization factor, g_o, can be established. For many sensors there is at least one atmospheric window band, typically in the 1500–2500 nm region, for which $B(\lambda) \approx 1$ (inspection of Fig. 1 shows that $B=0.9$ is a good estimate for typical clear atmospheric conditions); thus, for this band

$$g_o = 0.9 / \sigma\rho \tag{5}$$

If a suitable window band is not available, the normalization factor, g_o, can still be extracted directly from the standard deviation curve. Two bands ($\lambda_2 > \lambda_1$) are selected which are outside of any water absorption region, insuring that the atmospheric extinction is due primarily to the aerosols. The ratio of the standard deviations of these bands is a direct measure of the difference in aerosol optical depth, τ, via,

$$-\ln \frac{\sigma\rho(\lambda_1)}{\sigma\rho(\lambda_2)} = \tau(\lambda_1) - \tau(\lambda_2) \tag{6}$$

Depending on the wavelengths of the selected bands, a generally small correction for molecular Rayleigh scattering may be required. For aerosols, the ratio of optical depths at two wavelengths is well approximated by the Ångström formula,

$$\frac{\tau(\lambda_1)}{\tau(\lambda_2)} = \left(\frac{\lambda_2}{\lambda_1}\right)^{\alpha}, \ (\alpha>0) \qquad \textbf{(7)}$$

Combining Eqs. (6) and (7) allows one to convert the optical depth difference to an absolute optical depth at either wavelength,

$$\tau(\lambda_2) = \frac{-\ln\dfrac{\sigma\rho(\lambda_1)}{\sigma\rho(\lambda_2)}}{\left(\dfrac{\lambda_2}{\lambda_1}\right)^{\alpha} - 1}. \qquad \textbf{(8)}$$

The normalization factor is now determined from

$$g_o=\exp(-\tau(\lambda_2))/\sigma\rho(\lambda_2) \qquad \textbf{(9)}$$

It is noted that Eq. (9) is just a generalization of Eq. (5).

If neither the sensor radiometric calibration nor the solar illumination intensity is known, then $\sigma\rho$ is known only to within a scale factor and the normalization factor, g_o, must be estimated by a different method. One method is to set g_o such that that the maximum retrieved reflectance value for any wavelength and pixel is unity. This method is found to work reasonably in images containing a variety of man-made materials, such as urban scenes. Another method is to derive g_o by comparing the retrieved reflectance values with those in a library of material spectra.

For most scenes, the baseline curve is defined as the darkest observed signal for each band from among the diverse spectra. The presence of sufficiently dark pixels is indicated by at least one pixel spectrum with an apparent reflectance below ~0.05 for λ>1500 nm. For the rare situation that a dark spectrum is unavailable, it is still possible to estimate a reasonable background. One such method is to use a radiative-transfer code such as MODTRAN (Berk *et al.*, 1989, 1998; Acharya *et al.*, 1999) to compute the baseline based on the retrieved aerosol and molecular optical properties.

While the focus of the previous discussion was on atmospheric compensation, it was noted that QUAC provides, to within a normalization factor, the sun-surface-sensor path transmittance, $B(\lambda)$, which in window regions provides the wavelength-dependent aerosol extinction curve. The process flow for retrieving the aerosol optical properties is highlighted in Figure 4. Analysis of B can provide quantitative measures (column amounts) of all the atmospheric attenuation sources, including aerosol scattering and absorption, molecular absorption, and Rayleigh scattering. This may be accomplished through spectral fitting with an accurate atmospheric radiative-transfer code (e.g., MODTRAN) or, alternatively, by analytical approximations such as the Ångström law discussed above.

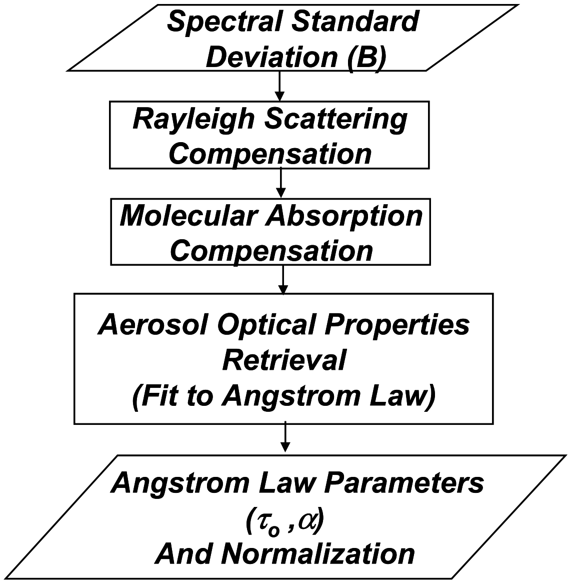

Figure 4. Overview of QUAC aerosol properties retrieval process flow.

Noting that the definition of a scene or image is flexible, the QUAC approach may be applied to individual sub-sections of a scene or image, if a sufficient diversity of pixel spectra exists within the sub-sections for computing a meaningful standard deviation and baseline. In this way, spatial variations in the adjacency-averaged reflectance $<\rho>$ and in the atmospheric parameters can be identified and taken into account in the atmospheric correction.

3.0 DATA ANALYSIS

QUAC was used to perform atmospheric correction and aerosol property retrieval on two very different hyperspectral AVIRIS (224 spectral channels from 400 to 2500 nm) data collects. As depicted in Figure 5, one corresponds to high visibility and low humidity, and the other to low visibility and high humidity. The NASA Stennis data is particularly useful because the Stennis site contains a large number of ground truth materials/panels (these are visible in the lower left corner of Figure 5).

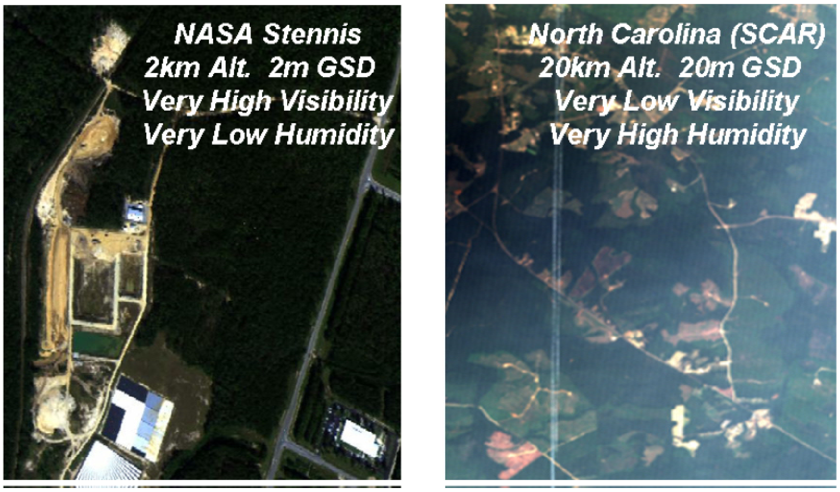

Figure 5. RGB image of the AVIRIS data sets used for evaluation of QUAC.

The first step in the process is the selection of diverse pixel spectra. For this analysis, we used the fast and automated SMACC (Sequential Maximum Angle Convex Cone) (Gruninger *et al.*, 2001) endmember code. To further speed the endmember-finding we used only ten window region wavelengths. The results for the NASA Stennis scene are displayed in Figure 6. It is evident that this set spans a wide variety of spectral shapes and reflectance values. Several endmembers are quite dark, and the lowest reflectance value for each channel defines the baseline spectrum.

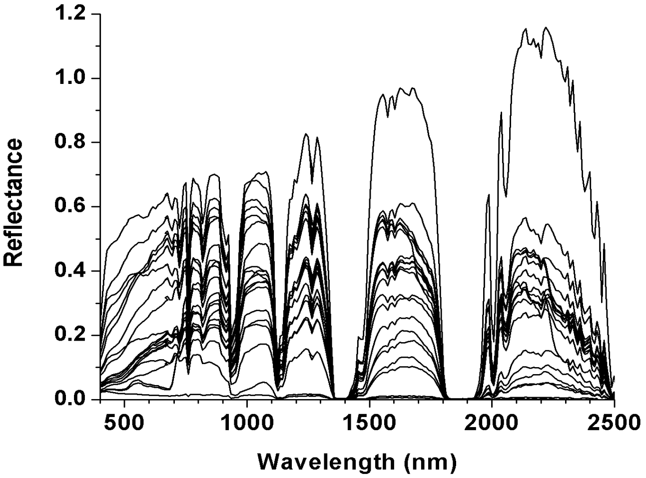

Figure 6. The first 20 endmembers selected by SMACC using the apparent reflectances from the NASA Stennis data.

The next step is to compute the standard deviation of the selected pixels. Before this is done, some refining of the initial selection usually occurs. This involves weeding out spectra with sharp features, mainly vegetation spectra that display a steep rise around 700 nm (the chlorophyll red edge). Pixels containing cirrus clouds, which can be easily discerned using established algorithms, are also rejected. The standard deviations for the NASA Stennis and North Carolina SCAR data are presented in Figure 7. The absorption due to the 940 nm H_2O band is clearly evident, and the much deeper feature seen in the North Carolina data is indicative of a much higher humidity level. Additional, weaker absorption features, such as the 840 nm H_2O and 760 nm O_2 bands are easily discernible. The general upper bounding envelope to these curves, formed by spectral regions outside of the absorption features, is a direct measure of the aerosol extinction for the L-shaped path from the sun to the surface to the sensor (i.e., the *B* coefficient). By inspection, it is quite obvious that the Stennis scene corresponds to a high visibility while the North Carolina scene displays approximately an order of magnitude more aerosol extinction and corresponds to a much lower visibility. The aerosol extinction is quantified below.

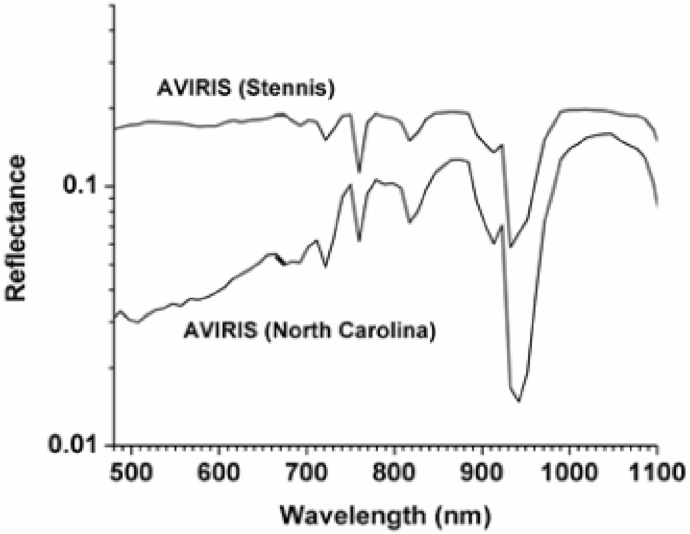

Figure 7. Spectral standard deviations based on the selected endmembers for the Stennis and North Carolina AVIRIS data sets.

From the above information, baseline and standard deviation, the entire data cube can be atmospherically corrected. Sample results for the Stennis data are shown in Figure 8 and include comparisons to FLAASH (Matthew *et al.* 2003, 2000) results and ground truth measurements. In this instance, and in general, QUAC compares well to FLAASH. The computational time required for the end-to-end QUAC process for an entire AVIRIS data cube (512 x 512 pixels and 224 spectral channels), as defined in Figure 8, is ~1 min on a 1.6 GHz Pentium IV PC. This is based on relatively slow IDL coding for the endmember selection and atmospheric correction steps. For comparison, FLAASH, which run a series of MODTRAN calculations, requires ~10min to perform the atmospheric correction.

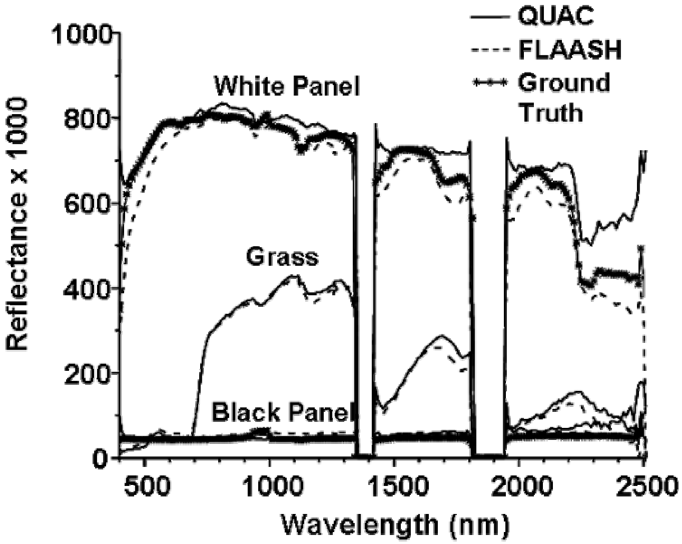

Figure 8. Comparison of QUAC atmospherically-corrected reflectances to those obtained from FLAASH and ground truth measurements for the Stennis data.

The key underlying assumption for QUAC is that the standard deviation of the endmember reflectances is independent of wavelength. This can be demonstrated by considering the FLAASH-corrected endmembers selected above by SMACC for the Stennis scene. It is noted that we cannot use the QUAC corrected endmembers since the assumption of a flat standard deviation is built into the approach, and in fact the standard deviation of the QUAC-corrected endmembers will be absolutely constant. However, no such assumption is built into FLAASH. The results are depicted in Figure 9. The effect of refining the endmember selection to weed out vegetation and outliers (exceptionally bright pixels and glints) is also shown in Figure 9. We ascribe the non-flat behavior on the edges to possible calibration issues and/or imperfect atmospheric correction. In any event, for most of the spectral regime, ~500–2400 nm, the standard deviation is acceptably flat. We have produced similar curves for a number of different AVIRIS data sets and find similarly good, and sometimes better, behavior of the standard deviations.

An advanced implementation of QUAC could correct for the residual errors associated with the deviation from perfectly flat spectral behavior for the endmember standard deviation. The underlying assumption is that the basic QUAC approach yields a sufficiently good atmospheric correction to allow for a useful un-mixing of the corrected endmember spectra based on a material spectral library. The standard deviation may be computed for the library fit to the endmember spectra, and the resulting standard deviation curve from this fit used to further improve the atmospheric correction.

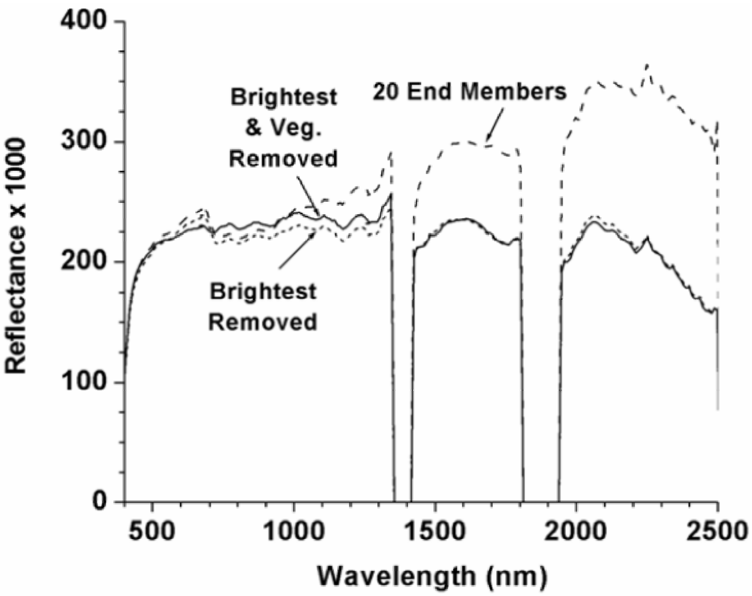

Figure 9. Standard deviation of the FLAASH-corrected endmembers for the Stennis scene.

QUAC was also applied to the multispectral satellite-based LANDSAT ETM+ sensor (6 broad bands, 450–2500 nm, 30 m GSD). The results with comparison to FLAASH are displayed in Figure 10.

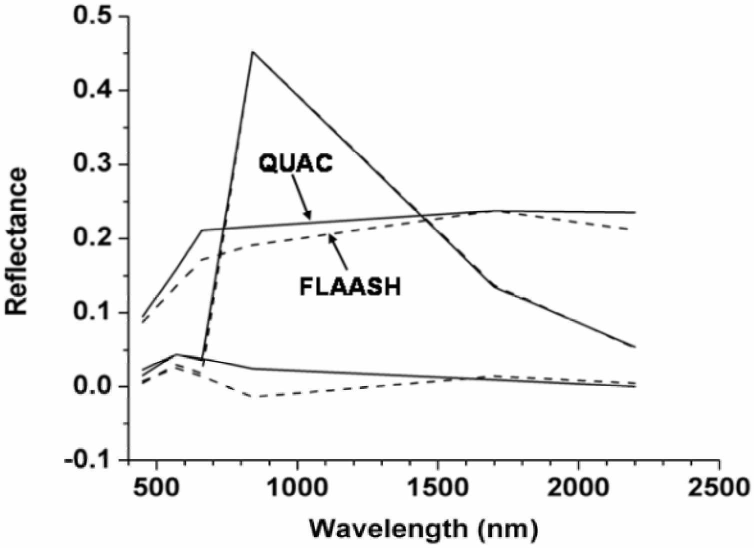

Figure 10. QUAC results and comparison to FLAASH for the multispectral LANDSAT ETM+ sensor.

The use of QUAC to retrieve aerosol optical properties following the process defined in Figure 4 is illustrated in Figure 11 for the Stennis and North Carolina data sets. An interesting result concerns the retrieved Ångström law exponent, α, which is indicative of aerosol type. For the North Carolina aerosol, α=1.5, which is identical to that for the MODTRAN rural aerosol model. For the Stennis data, α=2.4, which indicates a stratospheric aerosol type. This makes sense, as the small aerosol optical depth retrieved may all be attributed to a small residual stratospheric aerosol contribution as opposed to boundary layer aerosols.

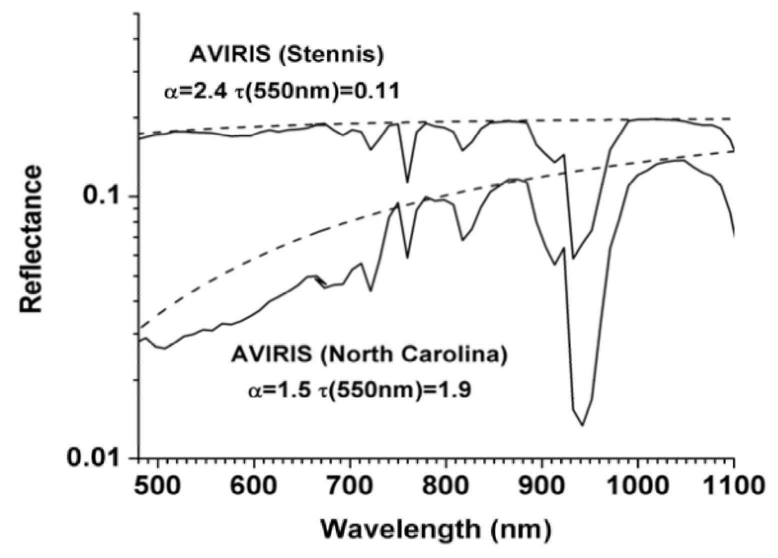

Figure 11. QUAC retrieval of aerosol optical properties based on an Ångström law fit (dashed lines) to the endmember standard deviations for the AVIRIS Stennis and North Carolina data sets.

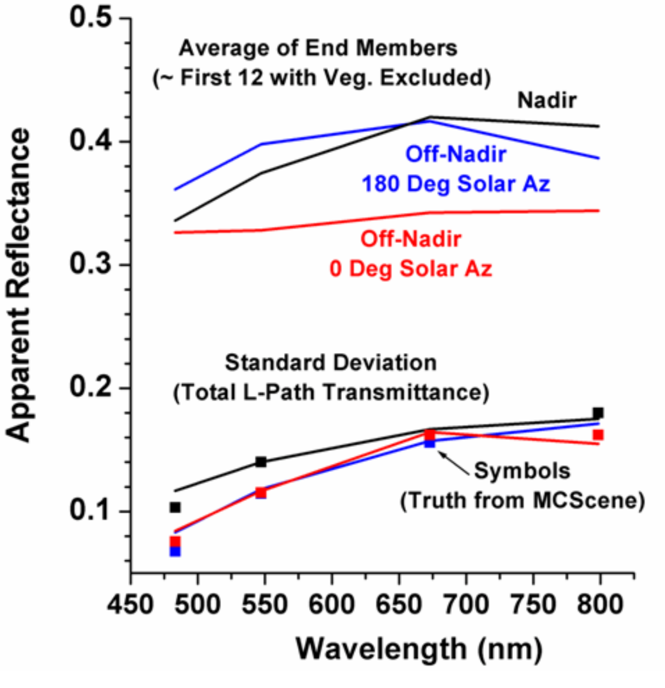

Figure 12. Average reflectances (top curves) and standard deviations (bottom curves) for the endmembers selected for the IKONOS simulation. The square symbols on the bottom curves are the actual $B(\lambda)$ values used in the simulations.

Validation of the QUAC aerosol property retrieval approach is considerably more difficult to accomplish than the atmospheric correction approach because it requires complete characterization of the aerosol vertical profile concurrent to an HSI or MSI data collection. In lieu of such data, the next best validation approach is to use a high-fidelity HSI or MSI simulation code. We have recently developed such a code (Berk *et al.*, 2000a; Richtsmeier *et al.*, 2001), called MCSCENE, for this purpose. Briefly, it features a backward Monte Carlo multiple-scattering radiative-transfer approach utilizing MODTRAN spectroscopy, includes a fully 3D voxelized atmosphere, and models the surface at high spatial resolution allowing for topographical features and BDRFs (Bi-Directional Reflectance Distribution Function). We performed simulations for the satellite-based IKONOS sensor (4 broad bands, 450–800 nm, 2 m GSD) of the Stennis site. This included nadir and off-nadir viewing and variation of the solar zenith angle (forward and backward aerosol scattering geometries). The Rural aerosol model with a visibility of 23 km was assumed. The results are presented in Figure 12. The QUAC derived aerosol optical properties are in close agreement with the actual ones used in the simulation. The off-nadir cases for the two solar azimuth/scattering geometries display very different average reflectances (higher for forward scattering – 180° azimuth) but identical aerosol transmittance curves, $B(\lambda)$. Even though the solar azimuths are quite different, the total L-shaped path lengths are identical and thus, should yield identical extinction curves.

4.0 CONCLUSIONS AND RECOMMENDATIONS

A new semi-empirical algorithm, QUAC, for atmospheric correction and aerosol optical properties retrieval for VIS-SWIR HSI and MSI sensors has been developed. Initial applications of QUAC to atmospheric correction of HSI AVIRIS and MSI LANDSAT data sets show surprisingly good performance, nearly comparable to that of a first-principles physics-based code. The utility of QUAC for retrieving wavelength-dependent aerosol extinction, and by extension aerosol type, was demonstrated for several AVIRIS data sets. An initial validation of the aerosol optical properties retrieval method was accomplished through the use of a HSI scene simulation approach. Continued development and validation of QUAC is recommended using a wider variety of HSI and MSI data sets, including simulated data, and through field measurements involving full characterization of the aerosol column concurrent with airborne and/or satellite-based HSI and MSI observations. Computational speed-ups, automation, and eventually the development of an on-board data processing capability should also be explored.

5.0 REFERENCES

Acharya, P.K., A. Berk, N.F. Larsen, S.-C. Tsay, and K.H. Stamnes, “MODTRAN4: multiple scattering and bidirectional reflectance distribution function (BRDF) upgrades to MODTRAN,” *SPIE 3756*, pp. 354–362, 1999.

Adler-Golden, S.M., M.W. Matthew, L.S. Bernstein, R.Y. Levine, A. Berk, S.C. Richtsmeier, P.K. Acharya, Anderson, G.P., G. Felde, J. Gardner, M. Hoke, L.S. Jeong, B. Pukall, J. Mello, A. Ratkowski and H.-H. Burke, “Atmospheric Correction for Short-wave Spectral Imagery Based on MODTRAN4,” *Summaries of the Eighth Annual JPL Earth Science Workshop*, JPL Publication 99-17, pp. 12–23, Jet Propulsion Laboratory, Pasadena, CA, 1999.

Berk, A., L.S. Bernstein, and D.C. Robertson, “MODTRAN: A Moderate-Resolution Model for LOWTRAN 7,” GL-TR-89-0122, Geophysics Directorate, Phillips Laboratory, Hanscom AFB, MA, 1989.

Berk, A., L.S. Bernstein, G.P. Anderson, P.K. Acharya, D.C. Robertson, J.H. Chetwynd and S.M. Adler-Golden, “MODTRAN Cloud and Multiple Scattering Upgrades with Application to AVIRIS,” *Remote Sens. Environ.*, 65, 367–375, 1998.

Berk, A., P.K. Acharya, S.M. Adler-Golden, and L.S. Bernstein, “A 3-D Hyperspectral Imagery Simulation Test Bed for the Littoral Zone - Phase I Final Report”, SSI-TR-356, Spectral Sciences, Inc., Burlington, MA, 2000a.

Berk, A., P.K. Acharya, L.S. Bernstein, G.P. Anderson, J.H. Chetwynd, and M.L. Hoke, “Reformulation of the MODTRAN band model for higher spectral resolution,” *SPIE Proceeding, Algorithms for Multispectral, Hyperspectral, and Ultraspectral Imagery VI, Vol. 4049*, pp. 190–198, 2000b.

Gao, B.-C. M. J. Montes, Z. Ahmad, and C.O. Davis, “Atmospheric Correction Algorithm for Hyperspectral Remote Sensing of Ocean Color from Space,” *Applied Optics,* 39, 887–896, 2000.

Gao, B.-C., K.B. Heidebrecht, and A.F.H. Goetz, “Derivation of Scaled Reflectances from AVIRIS Data,” *Proceedings of the Fourth Annual JPL Airborne Geoscience Workshop*, Vol. I. pp. 35–36, 1993.

Green, R.O., D.A. Roberts, and J.E. Conel, “Characterization and Compensation of the Atmosphere for Inversion of AVIRIS Calibrated Radiance to Apparent Surface Reflectance,” *Summaries of the Sixth Annual JPL Earth Science Workshop*, JPL Publication 96-4, Vol. 1, pp. 135–146, 1996.

Gruninger, J.H., M.J. Fox and R.L. Sundberg, “Hyperspectral Mixture Analysis using Constrained Projections onto Material Subspaces,” *Proceedings of the International Symposium on Spectral Sensing Research*, Québec City, pp. 162–170, 2001.

Kaufman, Y.J., A.E. Wald, L.A. Remer, B.-C. Gao, R.-R. Li and L. Flynn, “The MODIS 2.1-μm Channel-Correlation with Visible Reflectance for Use in Remote Sensing of Aerosol,” *IEEE Trans. Geosci. Remote Sens.*, 35, 1286–1298, 1997.

Kruse, F. A., K. S. Kierein-Young, and J. W. Boardman, “Mineral mapping at Cuprite, Nevada with a 63-channel imaging spectrometer,” *Photogrammetric Engineering & Remote Sensing*, 56, 83–92, 1990.

Matthew, M.W., S.M. Adler-Golden, A. Berk, G. Felde, G.P. Anderson, D. Gorodetzky, S. Paswaters and M. Shippert, “Atmospheric Correction of Spectral Imagery: Evaluation of the FLAASH Algorithm with AVIRIS Data,” *SPIE Proceeding, Algorithms and Technologies for Multispectral, Hyperspectral, and Ultraspectral Imagery IX*, 5093, pp. 474–482, 2003.

Matthew, M.W., S.M. Adler-Golden, A. Berk, S.C. Richtsmeier, R.Y. Levine, L.S. Bernstein, P.K. Acharya, G.P. Anderson, G.W. Felde, M.P. Hoke, A. Ratkowski, H.-H. Burke, R.D. Kaiser, and D.P. Miller, “Status of Atmospheric Correction Using a MODTRAN4-based Algorithm,” *SPIE Proceeding, Algorithms for Multispectral, Hyperspectral, and Ultraspectral Imagery VI*, *4049*, pp. 199–207, 2000.

Miller, C. J., “Performance assessment of ACORN atmospheric correction algorithm,” *SPIE Proceedings, Algorithms and Technologies for Multispectral, Hyperspectral, and Ultraspectral Imagery VIII*, 4725, pp. 438–449, 2002.

Montes, M.J., B.-C. Gao, and C.O. Davis, “A new algorithm for atmospheric correction of hyperspectral remote sensing data,” *SPIE Proceedings, Geo-Spatial Image and Data Exploitation II, Vol. 4383*, pp. 23–30, 2001.

Qu, Z., A.F.H. Goetz, and B. Kindel, “High-accuracy Atmospheric Correction for Hyperspectral Data (HATCH),” *Proceedings of the Ninth AVIRIS Earth Sciences and Applications Workshop*, JPL Publication 00-18, pp. 373–380, Jet Propulsion Laboratory, Pasadena, CA, 2000.

Richter, R. and D. Schlaepfer, “Geo-atmospheric processing of airborne imaging spectrometry data Part 2: atmospheric/topographic correction” *Int. J. Remote Sensing*, 23, 2631–2649, 2002.

Richtsmeier, S.C., A. Berk, S.M. Adler-Golden, and L.S. Bernstein, “A 3D Radiative-Transfer Hyperspectral Image Simulator for Algorithm Validation,” *Proceedings of the International Symposium on Spectral Sensing Research*, Québec City, 2001. (Inadvertently missing from proceedings – available as a pdf at www.spectral.com)

Roberts, D. A., Y. Yamaguchi, and R. J. P. Lyon, “Calibration of Airborne Imaging Spectrometer data to percent reflectance using field spectral measurements,” *19th International Symposium on Remote Sensing of Environment*, Ann Arbor, MI, 1985.

6.0 ACKNOWLEDGEMENTS

Spectral Sciences, Inc. efforts were funded through an AFRL Phase I SBIR project F19628-02-C-0054 with additional support provided via AFRL F19628-02-C-0078 and Spectral Sciences, Inc. IR&D activity.